Sandwich Beams With Corrugated and Y-frame Cores: Does the Back Face Contribute to the Bending Response?

L. St-Pierre

N. A. Fleck[1]
e-mail: naf1@eng.cam.ac.uk

V. S. Deshpande

Department of Engineering,
University of Cambridge,
Trumpington Street,
Cambridge, CP2 1PZ, UK

Stainless steel sandwich beams with a corrugated core or a Y-frame core have been tested in three-point bending and the role of the face-sheets has been assessed by considering beams with (i) front-and-back faces present, and (ii) front face present but back face absent. A fair comparison between competing beam designs is made on an equal mass basis by doubling the front face thickness when the back face is absent. The quasi-static, three-point bending responses were measured under simply supported and clamped boundary conditions. For both end conditions and for both types of core, the sandwich beams containing front-and-back faces underwent indentation beneath the mid-span roller whereas Brazier plastic buckling was responsible for the collapse of sandwich beams absent the back face. Three-dimensional finite element (FE) predictions were in good agreement with the measured responses and gave additional insight into the deformation modes. The FE method was also used to study the effect of (i) mass distribution between core and face-sheets and (ii) beam span upon the collapse response of a simply supported sandwich panel. Sandwich panels of short span are plastically indented by the mid-span roller and the panels absent a back face are stronger than those with front-and-back faces present. In contrast, sandwich panels of long span undergo Brazier plastic buckling, and the presence of a back face strengthens the panel.
[DOI: 10.1115/1.4004555]

Keywords: sandwich beam, Y-frame core, corrugated core, three-point bending

1 Introduction

Oil tanker spills pose a significant environmental threat to the oceans and coastlines of the world: 60% of worldwide oil transportation is by tankers and many heavily trafficked routes pass through regions of high marine biodiversity [1]. The conventional double hull design, with minimal mechanical coupling between inner and outer hulls, is commonly used to safeguard oil tankers against spills. Recently, design alternatives have been proposed to improve the structural performances of ship hulls over those normally achieved with a conventional double hull construction, see for example the review by Paik [2]. One such alternative is to employ a sandwich construction to increase the stiffness, strength and energy absorption of the hull.

An example of sandwich construction is the Y-frame double hull design, as proposed by Damen Schelde Naval Shipbuilding[2] and as illustrated in Fig. 1(*a*). Full-scale collision tests have been performed on this structure and its resistance to tearing was found to exceed that of a conventional double hull design [3]. In these collision trials, the inner hull played a minor role and underwent negligible plastic deformation. This motivated the development of a single hull structure where the Y-frame stiffeners are welded directly to the bulkheads as shown in Fig. 1(*b*). Full-scale collision tests have also been performed on this single hull Y-frame structure. It has similar crash-worthiness to the Y-frame double hull design, but it is significantly simpler and cheaper to manufacture. Several inland waterway tankers have been manufactured using the Y-frame single hull design [4]. The corrugated core, under the trade-name Navtruss[3], is a competing design to the Y-frame. No large-scale collision tests on the Navtruss design have been reported in the open literature, and little is known about its crash-worthiness relative to that of the Y-frame core.

The relative performance of corrugated and Y-frame cores has been explored recently for a range of loadings in a laboratory setting. For example, the out-of-plane compressive strength and longitudinal shear strength of the Y-frame core and corrugated core have been investigated by Rubino et al. [5] and Côté et al. [6], respectively. The three-point bending response of sandwich beams with a corrugated core was studied by Valdevit et al. [7]; they proposed failure maps for simply supported beams. This work was extended by Rubino et al. [8] who compared the three-point bending responses of sandwich beams with a corrugated core and a Y-frame core under both simply supported and clamped boundary conditions. It was found that sandwich beams with a corrugated core or a Y-frame core have comparable responses on an equal mass basis. However, these studies have been limited to sandwich beams with identical front-and-back faces.

The objective of the current study is to explore the sensitivity of the three-point bending response of a sandwich beam to the relative placement of material in the core, front face and back face. The relative allocation of material can be represented in a diagram resembling a triple phase diagram, as shown in Fig. 2. Any point on this diagram corresponds to a sandwich structure of total areal mass m, with fraction (m_c/m) in the core, (m_f/m) in the front face and $(m_b/m) = 1 - (m_f/m) - (m_c/m)$ in the back face.

Our study focuses on two trajectories in the design space of Fig. 2. The first one is indicated by the vertical dashed line and includes all sandwich beams with identical front-and-back faces,

[1]Corresponding author. Tel: +44 1223 748240 Fax: +44 1223 332662 Email: naf1@eng.cam.ac.uk

[2]Damen Schelde Naval Shipbuilding, Glacisstraat 165, 4381 SE Vlissingen, Netherlands.

Contributed by the Applied Mechanics Division of ASME for publication in the JOURNAL OF APPLIED MECHANICS. Manuscript received February 1, 2011; final manuscript received June 25, 2011; published online November 14, 2011. Editor: Robert M. McMeeking.

[3]Astech Engineering Products Inc., 3030 Red Hill Ave., Santa Ana, CA 92705.

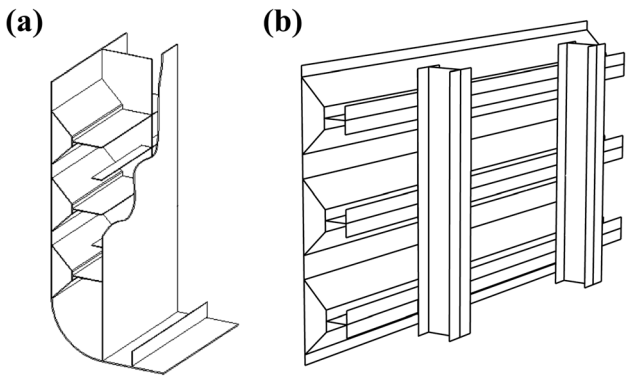

Fig. 1 The Y-frame sandwich core in (*a*) double hull and (*b*) single hull designs

$m_f = m_b$. The second trajectory is the left-hand edge of the triangle and denotes all sandwich beams absent the back face, $m_b = 0$.

The three-point bending response of sandwich panels of geometry along these two trajectories will be compared on an equal mass basis. Consider, as the reference design, a sandwich panel with identical front-and-back faces. If the back face material is relocated to the front face or to the core, will the three-point bending strength increase or decrease? This question is now addressed for a corrugated core and a Y-frame core, and for both simply supported and clamped boundary conditions.

1.1 Choice of Test Material. There is a need to select a pertinent test material, which in the as-manufactured state has similar properties to that of commercial shipbuilding steel, such as Lloyd's Grade A steel. The uniaxial tensile response of Lloyd's Grade A steel has been measured by Broekhuijsen [9] and is shown in Fig. 3. It is used by Damen Schelde Naval Shipbuilding in the construction of tankers with a Y-frame sandwich core.

In previous laboratory studies [5–8] corrugated cores and Y-frame cores have been manufactured by brazing together AISI 304 stainless steel sheets. In order to compare the uniaxial properties of this material with those of Lloyd's Grade A steel, preliminary uniaxial tests have been performed on dog-bone specimens cut from as-received AISI 304 stainless steel sheets; these were subjected to the same braze cycle as that used in the manufacture of sandwich beams (see Sec. 2.1). The uniaxial tensile response of the brazed 304 material, at an applied strain rate of 10^{-3} s^{-1}, is included in Fig. 3. The measured Young's modulus E and 0.2% offset yield strength σ_Y are 210 GPa and 210 MPa, respectively. The observed strain hardening response is close to linear, with a tangent modulus of $E_t = 2.1$ GPa. Lloyd's Grade A steel has a slightly higher yield strength of 280 MPa and a somewhat reduced ductility and strain hardening capacity. In broad terms, however, the as-brazed stainless steel is representative of Lloyd's grade A steel at strain levels below 10%. To confirm this, a limited set of finite element simulations have been performed on the three-point bending response of sandwich beams made from as-brazed stainless steel and Lloyd's grade A steel, as summarized in the Appendix. The simulations confirm that sandwich beams made from as-brazed stainless steel or from Grade A steel have similar responses. Based upon these exploratory findings, the sandwich beams of the present study were manufactured by brazing together type 304 stainless steel sheets.

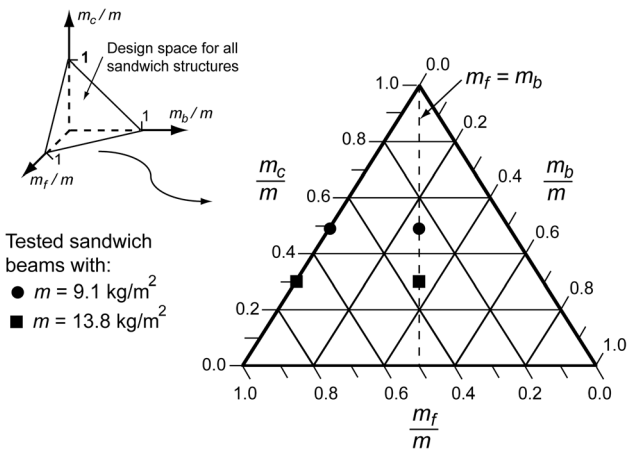

Fig. 2 The design space for mass distribution within a sandwich panel of areal mass *m*. The proportion of mass in the core, in the front face and in the back face are denoted by m_c/m, m_f/m and m_b/m, respectively. The mass distribution of the test geometries is indicated for two choices of areal mass.

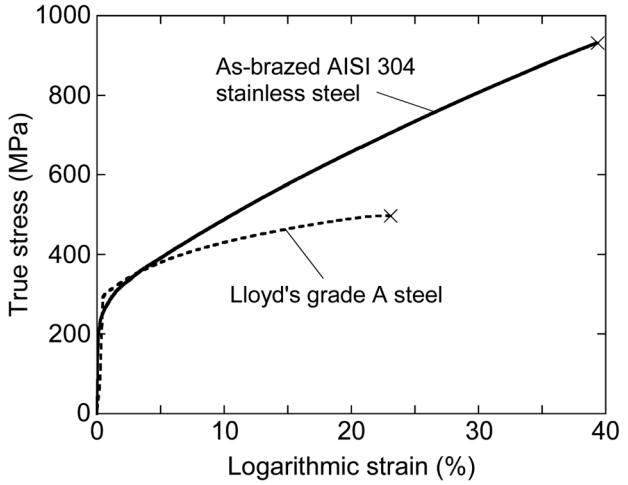

Fig. 3 Measured uniaxial tensile responses of as-brazed AISI 304 stainless steel and Lloyd's Grade A steel, at a strain rate of 10^{-3} s^{-1}

1.2 Scope of Study. First, the methodology used to manufacture and test the sandwich beams is reported along with a description of the finite element models. Second, the measured three-point bending responses of sandwich beams, with and without a back face, are compared for simply supported and clamped boundary conditions. Then, to gain additional insight into the collapse mechanisms, the beam responses are simulated by a three-dimensional finite element analysis. Finally, the three-point bending response of simply supported sandwich panels is explored numerically as a function of span and of relative proportion of material in the core and face-sheets. The two asymptotic responses of indentation at short span and a bending instability at long span are analyzed and used to determine the collapse load as a function of span.

2 Methodology

2.1 Specimen Manufacture. Corrugated and Y-frame cores, of cross section shown in Fig. 4, were used to construct prismatic sandwich beams. These cores are approximately 1:20 scale models of the cores used in a ship hull and had a relative density of 2.5%. Both cores were made from AISI 304 stainless steel sheets of thickness 0.3 mm and density $\rho = 7900$ kg/m^3.

The corrugated core was manufactured by alternately folding stainless steel sheets at ±60 deg under computer-numerical-control (CNC). In contrast, the Y-frame core was manufactured by CNC folding of stainless steel sheets and then assembling two sections: the ±45 deg upper part of the Y-frame and the Y-frame leg. Slots were cut periodically into the central flange of the upper part of the Y-frame and a matching set of keys were cut into the top of

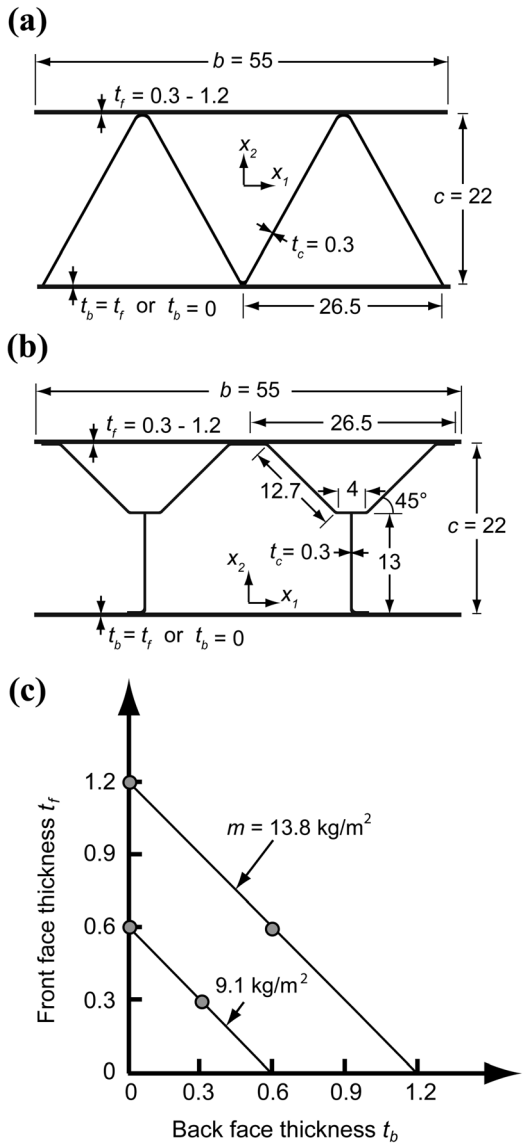

Fig. 4 Cross-sectional dimensions of the sandwich beams: (*a*) corrugated core and (*b*) Y-frame core. (*c*) The chosen values of face-sheet thickness used in the experimental study. All dimensions are in mm.

the Y-frame leg to facilitate assembly, as described by Rubino et al. [5].

Stainless steel face-sheets were brazed to the cores to produce two classes of sandwich beam:

(i) a beam with front-and-back faces of thickness t and
(ii) a beam with only a front face of thickness $2t$.

Two different values of thickness t were considered, 0.3 mm and 0.6 mm, giving sandwich beams of areal mass $m = 9.1$ kg/m^2 and 13.8 kg/m^2, respectively, as shown in Fig. 4(*c*). These test geometries are also included in the design space of Fig. 2. The proportion of mass in the core m_c/m is 0.48 and 0.31 for the sandwich beams of areal mass m of 9.1 kg/m^2 and 13.8 kg/m^2, respectively.

The sandwich beams were assembled as follows. First, the face-sheets were spot-welded to the core, and second, a thin layer (of thickness 10 μm) of Ni-CR 25-P10 (wt.%) braze powder was applied over all sheets of the assembly. Third, brazing was performed in a vacuum furnace (at 0.03–0.1 mbar) using a dry argon atmosphere at 1075°C for 1 h, followed by a slow furnace cool.

2.2 Geometry of the Three-Point Bending Tests. Simply supported and clamped sandwich beams were employed, of dimensions shown in Fig. 5. In all cases, the prismatic axis of the core was aligned with the longitudinal direction of the beam (x_3-axis). The span of the beams was held fixed at $2L = 250$ mm and load introduction at mid-span was via a steel roller of diameter $D = 9$ mm.

2.2.1 Simply Supported Beams. Steel rollers of diameter $D = 9$ mm were also used to provide simple outer support to the sandwich beams, see Fig. 5(*a*). For those specimens without a back face, preliminary tests revealed that the core crushed and splayed out-of-plane (in the x_1-direction) at the outer supports. To prevent this mode of collapse, short sections of back face were brazed to the core at both ends of the beam (see Fig. 5(*a*)). These additional face plates had the same thickness as that of the front face-sheet. No such reinforcement was required for the sandwich beams with front-and-back faces.

2.2.2 Clamped Beams. To achieve a fully clamped boundary condition, the ends of the sandwich beams were filled with an epoxy resin to make the core fully dense. Then, the end portions of the sandwich beams were bolted to the test rig using steel clamping plates and M6 bolts, as shown in Fig. 5(*b*). For those specimens absent the back face, local reinforcement was again achieved by brazing short sections of back face to the core at each end of the beam.

2.3 Finite Element Models. The commercial software Abaqus was used to develop three-dimensional finite element (FE) models for all sandwich beams tested. The geometries used in the simulations were identical to those employed in the experimental investigation, recall Figs. 4 and 5. Perfect bonding between core and face-sheets was assumed in all cases. Four noded, linear shell elements with reduced integration (S4R in Abaqus notation [10]) were used to discretize the sandwich beams using a mesh size of 0.5 mm. A convergence study showed that further mesh refinement did not improve significantly the accuracy of the simulations.

2.3.1 Boundary Conditions. Only one quarter of the sandwich beam was modeled in the simulations, with symmetric boundary conditions at mid-span ($x_3 = 0$) and at midplane ($x_1 = 0$). The mid-span roller was modeled as a rigid body in the FE simulations and its displacement was prescribed during the analysis. A frictionless hard contact condition was used to model the interaction between the roller and front face. The same contact properties were used between all potentially contacting surfaces of the sandwich beam.

The overhang of the simply supported sandwich beams beyond the outer rollers was included in the FE analysis. Alternatively, the clamped boundary condition was enforced by imposing zero displacement on the nodes of the end face of the sandwich beam ($x_3 = L$).

2.3.2 Material Properties. The as-brazed AISI 304 stainless steel was modeled as a rate-independent, elastic-plastic solid in accordance with J2-flow theory. The elastic branch was linear and isotropic, as characterized by a Young's modulus $E = 210$ GPa and a Poisson's ratio $\upsilon = 0.3$. The uniaxial yield strength was $\sigma_Y = 210$ MPa, and the hardening response was tabulated in Abaqus from the plot in Fig. 3.

3 Experimental Results

The three-point bending tests were conducted using a 100 kN screw driven test machine with a constant cross-head velocity of $\dot{\delta} = 5 \times 10^{-3}$ mm/s. The load F applied to the specimen was measured by the load cell of the test machine and the mid-span roller displacement δ was measured via a laser extensometer.

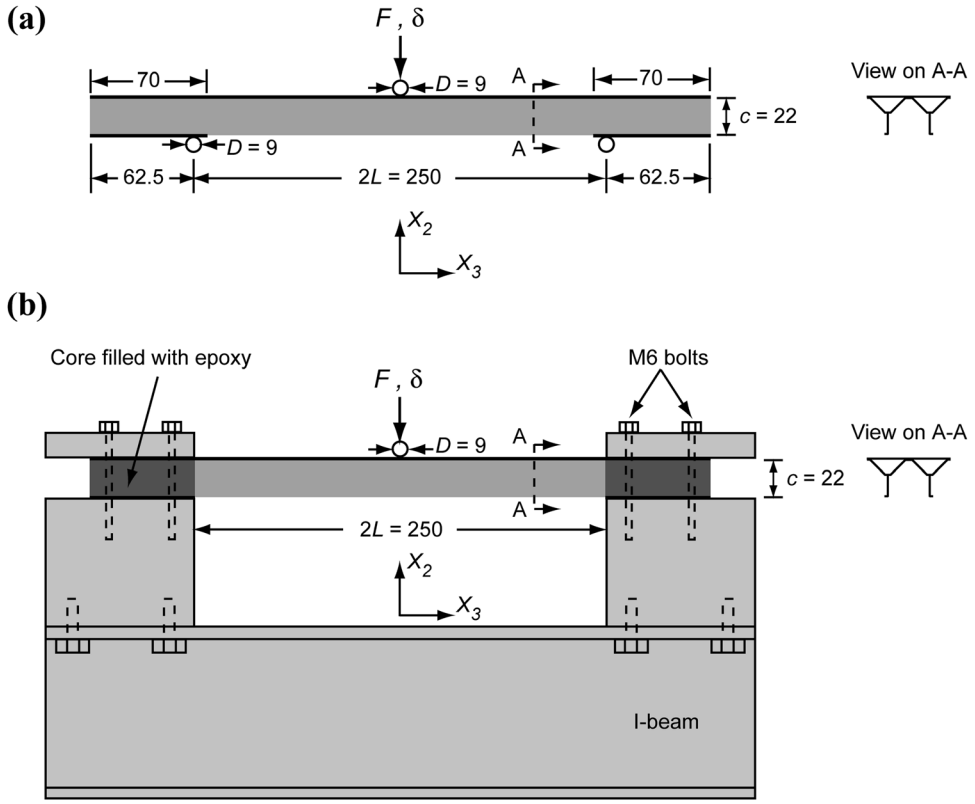

Fig. 5 The test fixtures used for (*a*) simply supported and (*b*) clamped beams. A sandwich beam with a Y-frame core and absent the back face is shown. All dimensions are in mm.

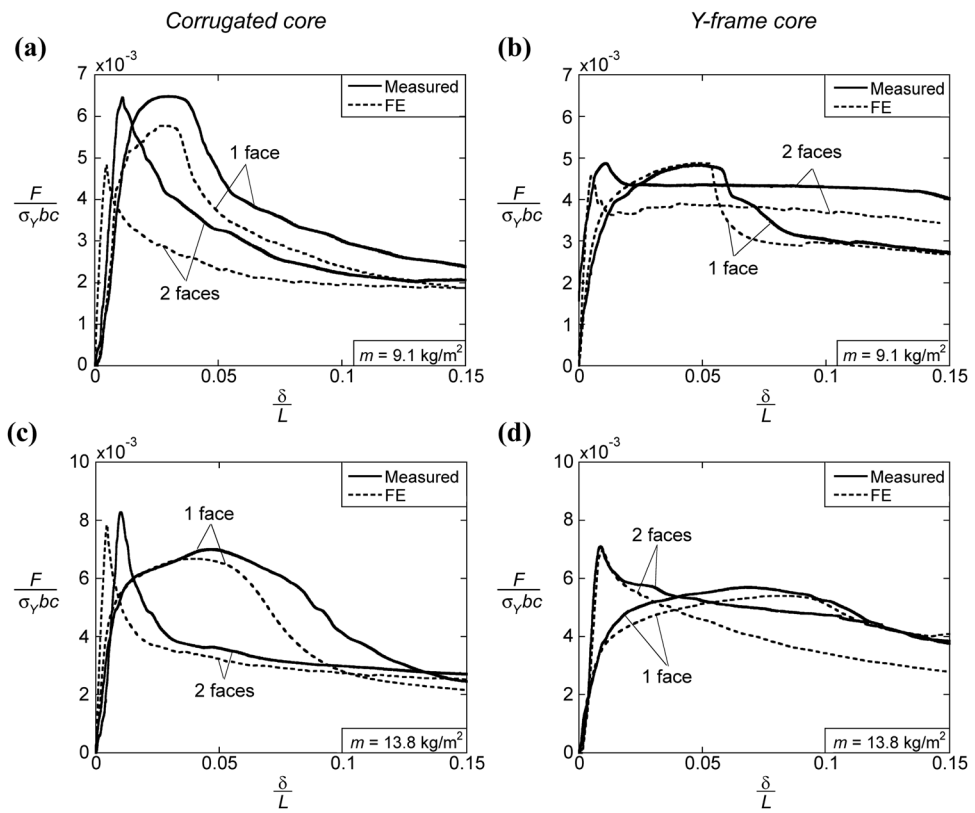

Fig. 6 Three-point bending responses of simply supported sandwich beams. Sandwich beams with an areal mass $m = 9.1$ kg/m^2 are shown with (*a*) a corrugated core and (*b*) a Y-frame core. Likewise, sandwich beams with an areal mass $m = 13.8$ kg/m^2 are shown with (*c*) a corrugated core and (*d*) a Y-frame core.

The three-point bending responses of all sandwich beams tested are given in Fig. 6 (simply supported) and in Fig. 7 (clamped boundary conditions). In each figure, results are shown for sandwich beams with a corrugated core and a Y-frame core, and for an areal mass $m = 9.1$ kg/m^2 and 13.8 kg/m^2. The mid-span roller displacement δ is normalized by the beam half-span $L = 125$ mm whereas the load F is normalized by $\sigma_Y bc$, where the yield strength is $\sigma_Y = 210$ MPa, the width of the sandwich beams is $b = 55$ mm and the core thickness is $c = 22$ mm.

3.1 Simply Supported Beams. The simply supported beam response is shown in Fig. 6(*a*) for the corrugated core and in Fig. 6(*b*) for the Y-frame core, both at $m = 9.1$ kg/m^2. Likewise, the response is given in Fig. 6(*c*) and 6(*d*) for the corrugated core and Y-frame core, respectively, at $m = 13.8$ kg/m^2. In each plot, results are shown for sandwich beams with both faces present and for sandwich beams with the back face absent.

All simply supported sandwich beams have an initial elastic regime. The elastic stiffness is, however, sensitive to the distribution of face-sheet material: beams containing both front-and-back faces are at least 40% stiffer than those with the back face absent. In contrast, the peak load reduces by less than 20% when the back face material is relocated onto the front face.

The peak load for sandwich beams with a corrugated core exceeds that of the beams with a Y-frame core by 15–25%. In all cases, the peak load is followed by a softening response, with more pronounced softening for the corrugated core than for the Y-frame core: the load drops to less than 35% of the peak load for sandwich beams with a corrugated core when δ/L is increased to 0.15. In contrast, for the Y-frame core the load at $\delta/L = 0.15$ exceeds 55% of the peak load.

3.2 Clamped Beams. The measured three-point bending responses of clamped sandwich beams are shown in Fig. 7. The layout of Fig. 7 is the same as that in Fig. 6: structures with a corrugated core and a Y-frame core are shown in Fig. 7(*a*) and 7(*b*), respectively, for an areal mass $m = 9.1$ kg/m^2. Likewise, the responses for $m = 13.8$ kg/m^2 are given in Fig. 7(*c*) and 7(*d*) for the corrugated core and Y-frame core, respectively. In each plot, the response of a sandwich beam with front-and-back faces present is compared to that of a sandwich beam absent the back face.

In all cases, an initial elastic regime is followed by a peak load F_{pk}. Subsequently, the clamped beams soften and then re-harden due to longitudinal stretching of the beam. The core topology has a similar influence upon the initial peak load of clamped beams to that of the simply supported beams: sandwich structures with a corrugated core are 10–25% stronger than their counterparts with a Y-frame core. The initial peak load of sandwich beams with an areal mass $m = 9.1$ kg/m^2 is sensitive to the distribution of face-sheet material: beams absent the back face are 25–35% stronger than those with front-and-back faces. In contrast, for $m = 13.8$ kg/m^2, the sandwich beams with front-and-back faces present have comparable initial peak strengths to those without a back face. For all clamped beams considered, the load drop following the initial peak load F_{pk} is at most 20%. We note in passing that the simply supported Y-frame core shows load drop of this order, whereas the corrugated core exhibits much larger load drops, recall Fig. 6.

3.3 Collapse Mechanisms. To gain additional insight into the collapse mechanisms, photographs of the deformed sandwich beams with an areal mass $m = 13.8$ kg/m^2 are shown in Figs. 8–11. Simply supported sandwich beams with a corrugated core and with

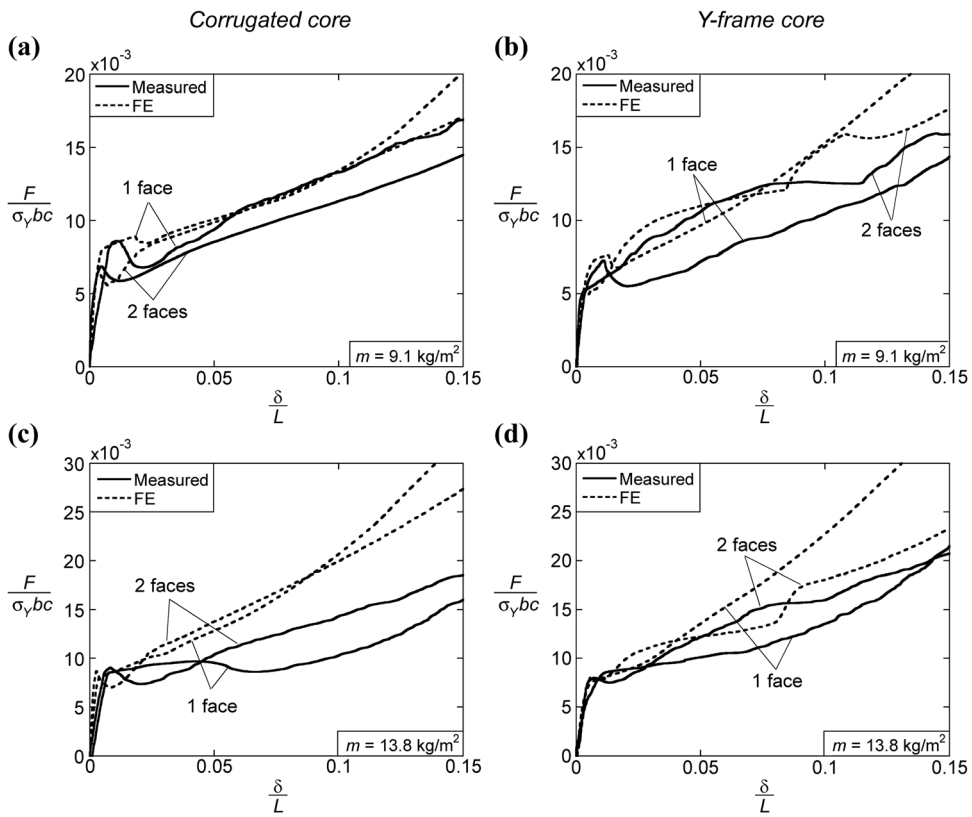

Fig. 7 Three-point bending responses of clamped sandwich beams. Sandwich beams with an areal mass $m = 9.1$ kg/m^2 are shown with (*a*) a corrugated core and (*b*) a Y-frame core. Likewise, sandwich beams with an areal mass $m = 13.8$ kg/m^2 are shown with (*c*) a corrugated core and (*d*) a Y-frame core.

a Y-frame core are given in Figs. 8 and 9, respectively. Likewise, photographs of clamped sandwich beams with a corrugated core and a Y-frame core are reported in Figs. 10 and 11, respectively. In part (*a*) of each figure, the deformed geometry is shown for front-and-back faces present, whereas in part (*b*) the images are for the back face absent. The photographs were taken after deforming the sandwich beam to $\delta = 0.2L$ and then unloading. Two views are shown in the figures: on the left, a side view along the x_3-direction showing half of the sandwich beam and on the right, a view of the core deformation after sectioning of the beam at mid-span.

The photographs of sandwich beams with front-and-back faces present, as shown in part (*a*) of Figs. 8–11, indicate that beam collapse is by indentation of the core beneath the mid-span roller. This holds true for both corrugated and Y-frame core topologies and for both simply supported and clamped beams. The normalized initial peak loads, $\bar{F} = F_{pk}/(\sigma_Y bc)$, for all sandwich beams tested are summarized in Table 1. It is clear from Table 1 that the initial peak load for indentation of sandwich beams with both faces present has only minor sensitivity to the choice of boundary conditions.

The images shown in part (*b*) of Figs. 8–11 reveal that the beams absent a back face collapse by plastic buckling at mid-span. This alternative mode is reminiscent of the buckling of circular tubes by ovalization of their cross section, as first identified by Brazier [11]. The progressive reduction of flexural plastic modulus of the sandwich beams in bending induces a Brazier-type instability, and we shall refer to this collapse mode by the generalized term "Brazier plastic buckling." The mode of Brazier plastic buckling is more diffuse than the highly localized indentation mode beneath the central roller, compare the images as given in parts (*a*) and (*b*) of Figs. 8–11.

The peak load F_{pk} associated with Brazier plastic buckling occurs at a significantly larger value of δ/L than the indentation mode for simply supported beams, recall Fig. 6. Also, the value of F_{pk} for Brazier plastic buckling is sensitive to the choice of boundary condition: the clamped beams are 30–50% stronger than simply supported beams (see Table 1). This is consistent with the fact that for a given applied load F, the bending moment at mid-span of clamped beams is less than that for simply supported beams.

4 Finite Element Predictions

A Finite Element (FE) investigation of the three-point bending response of sandwich beams with corrugated and Y-frame cores has been conducted with the following objectives:

(i) to obtain additional insight into the measured responses as presented in Sec. 3,
(ii) to explore the influence of mass distribution between core and face-sheets upon the three-point bending response of a sandwich panel, and
(iii) to analyze the effect of beam span upon the collapse mechanism.

All computations were performed using the commercial software Abaqus (version 6.9). Most simulations were done with the implicit solver, but the explicit solver was also used when convergence issues were encountered. The explicit solver can handle more easily the complex contact conditions that arise within the sandwich beam when the core is crushed beneath the mid-span roller. To ensure that a quasi-static solution was obtained with the

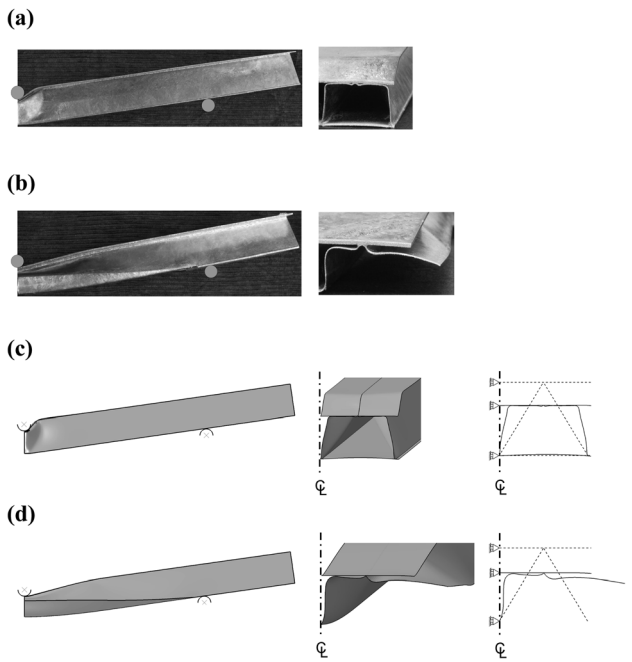

Fig. 8 Photographs of the simply supported sandwich beams with a corrugated core ($m = 13.8$ kg/m^2) (*a*) with front-and-back faces and (*b*) without a back face. Deformed finite element meshes of the same sandwich beam (*c*) with front-and-back faces and (*d*) without a back face. A side view showing half of the beam and a view of the core deformation at mid-span are given. To clarify the predicted deformation modes, the undeformed (dashed line) and deformed (solid line) cross sections at mid-span are included in Figs. 8(*c*) and 8(*d*). The images are for beams loaded to $\delta = 0.2L$ and then unloaded.

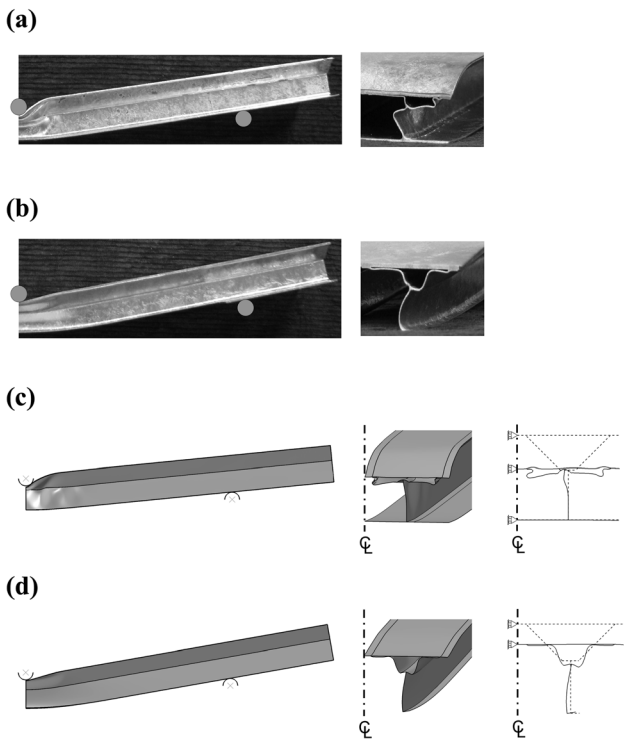

Fig. 9 Photographs of the simply supported sandwich beams with a Y-frame core ($m = 13.8$ kg/m^2) (*a*) with front-and-back faces and (*b*) without a back face. Deformed finite element meshes of the same sandwich beam (*c*) with front-and-back faces and (*d*) without a back face. A side view showing half of the beam and a view of the core deformation at mid-span are given. To clarify the predicted deformation modes, the undeformed (dashed line) and deformed (solid line) cross sections at mid-span are included in Figs. 9(*c*) and 9(*d*). The images are for beams loaded to $\delta = 0.2L$ and then unloaded.

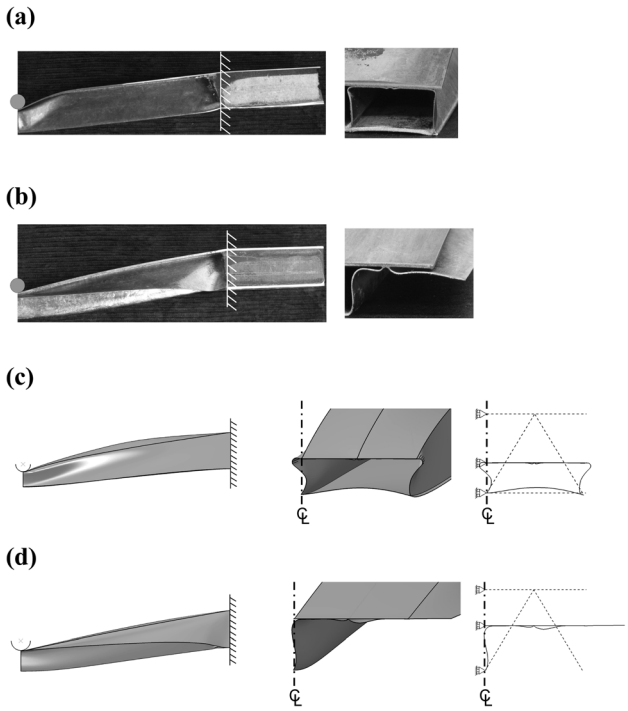

Fig. 10 Photographs of the clamped sandwich beams with a corrugated core ($m = 13.8$ kg/m^2) (*a*) with front-and-back faces and (*b*) without a back face. Deformed finite element meshes of the same sandwich beam (*c*) with front-and-back faces and (*d*) without a back face. A side view showing half of the beam and a view of the core deformation at mid-span are given. To clarify the predicted deformation modes, the undeformed (dashed line) and deformed (solid line) cross sections at mid-span are included in Figs. 10(*c*) and 10(*d*). The images are for beams loaded to $\delta = 0.2L$ and then unloaded.

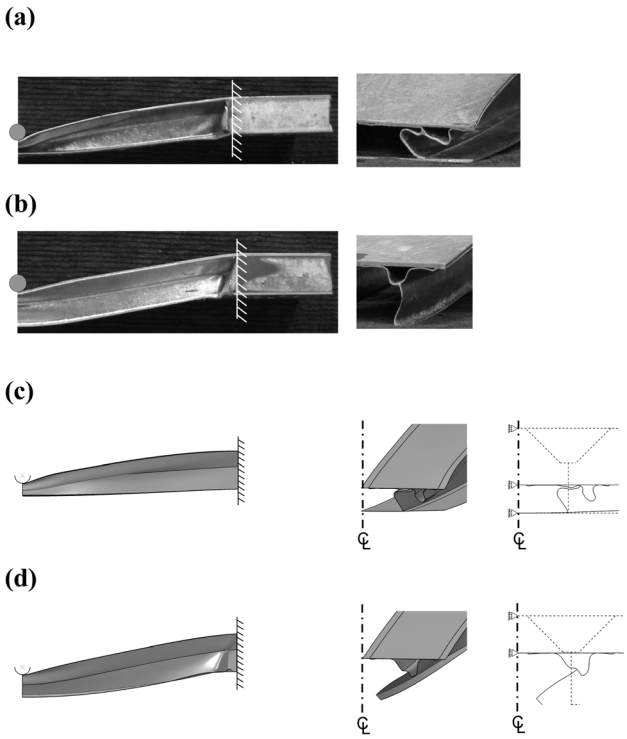

Fig. 11 Photographs of the clamped sandwich beams with a Y-frame core ($m = 13.8$ kg/m^2) (*a*) with front-and-back faces and (*b*) without a back face. Deformed finite element meshes of the same sandwich beam (*c*) with front-and-back faces and (*d*) without a back face. A side view showing half of the beam and a view of the core deformation at mid-span are given. To clarify the predicted deformation modes, the undeformed (dashed line) and deformed (solid line) cross sections at mid-span are included in Figs. 11(*c*) and 11(*d*). The images are for beams loaded to $\delta = 0.2L$ and then unloaded.

explicit solver, the kinetic energy of the sandwich beam was monitored to ensure it never exceeds 10% of the strain energy, as suggested within the Abaqus documentation [10].

4.1 Comparison Between Measurements and Simulations. The FE predictions for all sandwich beams tested are included in Figs. 6 and 7 for simply supported and clamped boundary conditions, respectively. In each figure, the simulated response of sandwich beams with a corrugated core (Figs. 6(*a*) and 7(*a*)) and a Y-frame core (Figs. 6(*b*) and 7(*b*)) is shown for $m = 9.1$ kg/m^2. Likewise, the results for sandwich beams with $m = 13.8$ kg/m^2 are shown with a corrugated core (Figs. 6(*c*) and 7(*c*)) and a Y-frame core (Figs. 6(*d*) and 7(*d*)).

It is evident from Fig. 6 that the predicted peak loads of the simply supported beams slightly underestimate the measured peak loads. This is attributed to the fact that the FE analysis assumes frictionless contact between the sandwich beam and rollers, and neglects the strengthening due to the presence of the braze alloy over all surfaces of the sandwich beam. In contrast, the FE

Table 1 The measured and predicted values of normalized peak load $\hat{F} = F_{pk}/(\sigma_Y bc)$

Specimen				$\hat{F} = \frac{F_{pk}}{\sigma_Y bc}(10^{-3})$	
Boundary condition	Areal mass (kg/m^2)	Core topology	Number of face-sheets	Measured	FE
Simply supported	9.1	Corrugated	1	6.5	5.8
			2	6.5	4.9
		Y-frame	1	4.8	4.9
			2	4.9	4.6
	13.8	Corrugated	1	7.0	6.6
			2	8.3	7.8
		Y-frame	1	5.7	5.4
			2	7.1	7.4
Clamped	9.1	Corrugated	1	8.6	9.0
			2	6.8	6.4
		Y-frame	1	7.2	7.6
			2	5.2	5.3
	13.8	Corrugated	1	9.6	10.2
			2	9.0	8.7
		Y-frame	1	8.7	7.7
			2	8.0	8.3

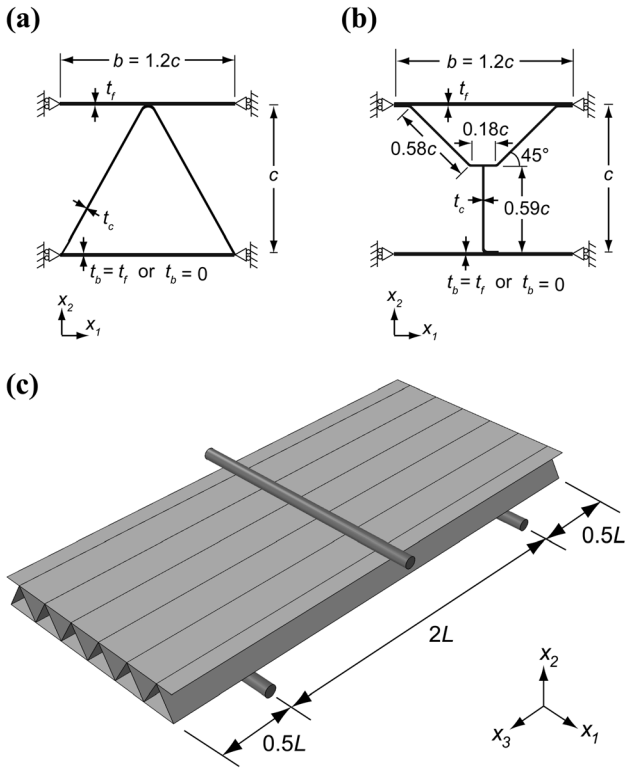

Fig. 12 Cross-sectional dimensions of the sandwich panels considered in the numerical analysis: (*a*) corrugated core and (*b*) Y-frame core. (*c*) The sandwich panels, shown here with a corrugated core, are simply supported and loaded in three-point bending.

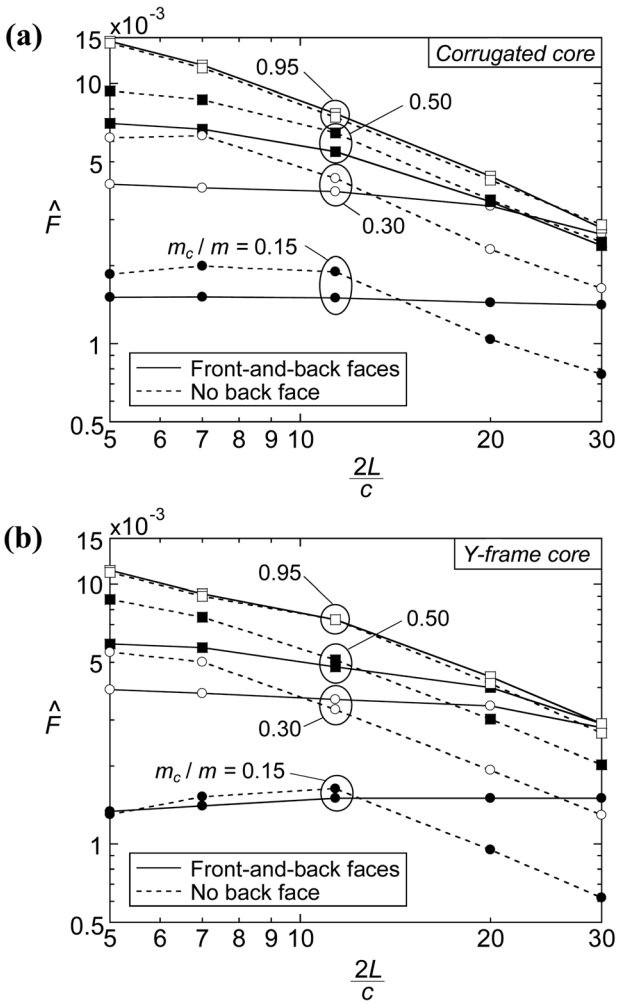

Fig. 13 Normalized peak load $\hat{F} = F_{pk}/(\sigma_Y bc)$ as a function of the normalized span $2L/c$ for simply supported sandwich panels and selected values of m_c/m ($m/\rho c = 0.052$). Results are shown for sandwich panels with (*a*) a corrugated core and (*b*) a Y-frame core.

analysis somewhat overpredicts the strength of the fully clamped beams following the initial peak load. This is traced to the fact that perfect clamping is assumed in the FE simulations whereas the test rig was unable to achieve this. The finite additional compliance of the test fixture is particularly significant for the sandwich beams of areal mass $m = 13.8$ kg/m^2 because the reaction force and moment at the supports is greater for these specimens.

The predicted shapes of deformed sandwich beams of areal mass $m = 13.8$ kg/m^2 are compared with photographs of the as-tested specimens in Figs. 8–11. Recall that simply supported beams with a corrugated core and a Y-frame core are shown in Figs. 8 and 9, respectively. Likewise, clamped beams with a corrugated core and a Y-frame core are given in Figs. 10 and 11, respectively. In each figure, beams with front-and-back faces present (part (*c*)) are compared with those absent the back face (part (*d*)). Additional views are included in parts (*c*) and (*d*) to show the predicted cross-sections at mid-span.

The observed and predicted deformation of the sandwich beams with front-and-back faces present is by indentation beneath the central roller. In contrast, for the sandwich beams absent the back face, the observed and predicted deformation mode is by Brazier plastic buckling at mid-span.

4.2 Sensitivity of the Sandwich Panel Response to Span and Proportion of Mass in the Core. In the experimental investigation presented in Sec. 3, the proportion of mass in the core and the span of the sandwich beams were held fixed. The sensitivity of collapse strength to these geometric parameters is now explored using the FE method. At this stage in the study, we change perspective from comparing FE predictions with the measured responses of sandwich *beams* to predicting the collapse response of sandwich *panels* in three-point bending. Sandwich panels are more commonly used in engineering practice (such as ship hulls) than sandwich beams, and it is of interest to evaluate the relative performance of corrugated cores and Y-frame cores in the sandwich panel configuration. We shall limit our attention to the simply supported case, and consider sandwich panels with identical front-and-back faces and panels with the back face absent. Results are presented in nondimensional form so that they are applicable over a wide range of length scales; from laboratory test to industrial application.

The cross sections of the sandwich panels are given in Fig. 12 for the corrugated core and Y-frame core. The panels are subjected to three-point bending, and are idealized by unit cells in the width-direction, as defined in Fig. 12. Under three-point bending, the panels will deform plastically over a limited portion along their length, and display negligible straining in the width direction, x_1. Consequently, the behavior of a panel of large width is adequately captured by considering the response of a unit cell with symmetric boundary conditions imposed along the sides, as shown in Fig. 12.

4.2.1 Dimensional Analysis. In the simulations, the core shape is held fixed and parameterized in terms of the core thickness c, as shown in Fig. 12. The relative mass distribution between core and face-sheets is dictated by the thickness of the core members and of the face-sheets according to the following prescription.

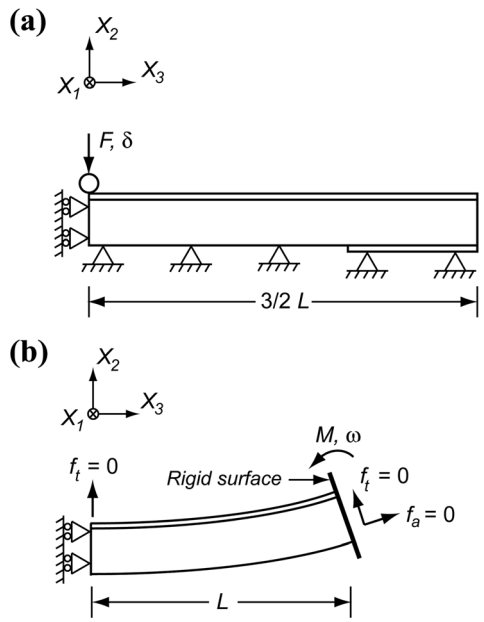

Fig. 14 The boundary conditions on FE models to simulate (*a*) indentation and (*b*) bending. A sandwich panel absent the back face is shown.

The areal mass of the core m_c scales with the thickness of the core members t_c according to

$$m_c = A\rho t_c \tag{1}$$

where the constant of proportionality is $A = 1.843$ for both corrugated core and Y-frame core. Likewise, the areal mass of the sandwich panel m scales with the thickness of the face-sheets t_f according to

$$m = \rho t_f + m_c \tag{2}$$

when the back face is absent and as

$$m = 2\rho t_f + m_c \tag{3}$$

when both front-and-back faces are present. Now, Eq. (1) can be rewritten in nondimensional form as

$$\frac{t_c}{c} = \frac{1}{A}\frac{m_c}{m}\frac{m}{\rho c} \tag{4}$$

and likewise Eqs. (2) and (3) can be re-arranged to the form

$$\frac{t_f}{c} = \left(1 - \frac{m_c}{m}\right)\frac{m}{\rho c} \tag{5}$$

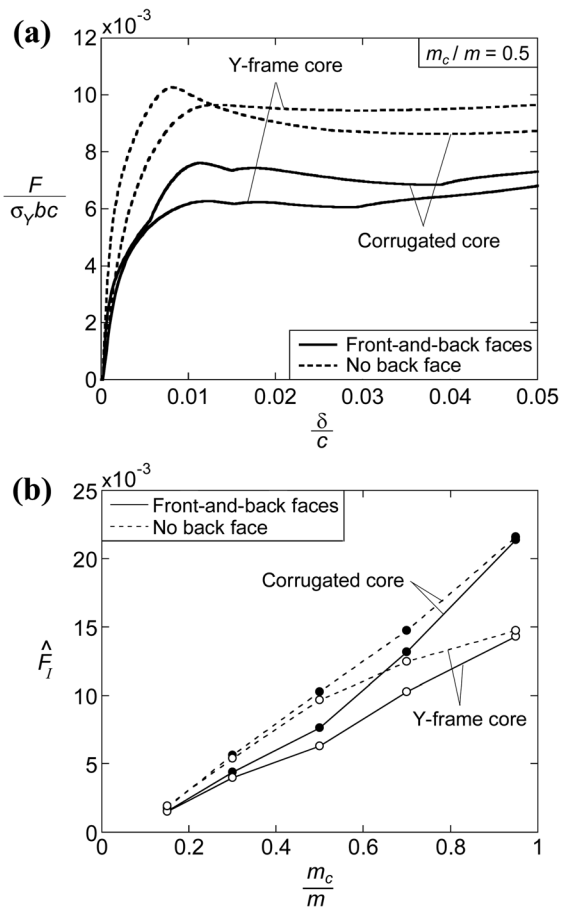

Fig. 15 (*a*) The predicted indentation response of sandwich panels with $m_c/m = 0.5$ resting on a rigid foundation. (*b*) Normalized indentation strength $\hat{F}_I = F_I/(\sigma_Y bc)$ as a function of m_c/m ($m/\rho c = 0.052$).

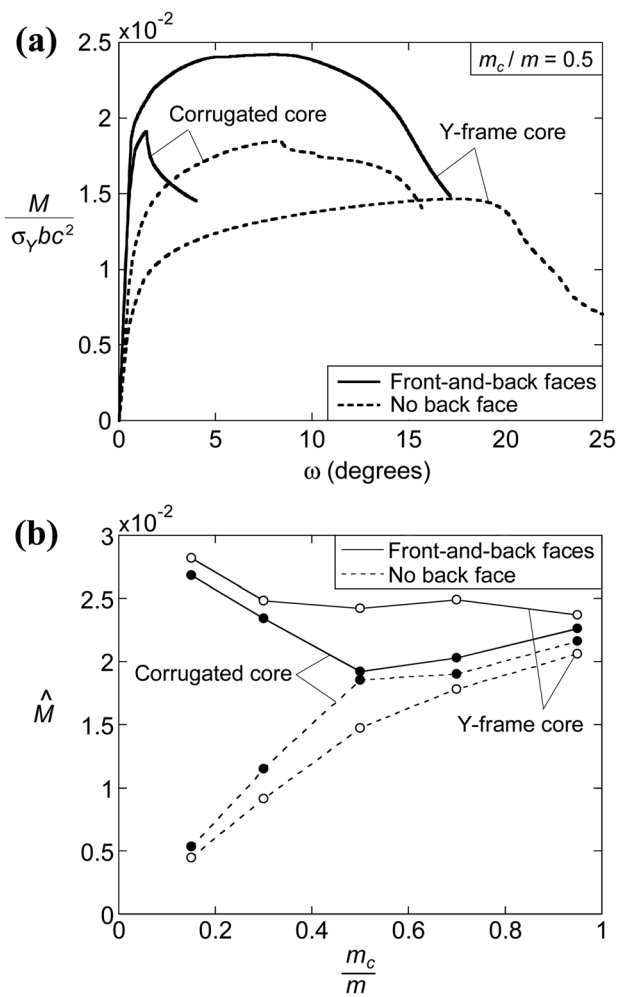

Fig. 16 (*a*) The predicted bending response of sandwich panels with $m_c/m = 0.5$. (*b*) Normalized Brazier buckling moment $\hat{M} = M_B/(\sigma_Y bc^2)$ as a function of m_c/m ($m/\rho c = 0.052$).

$$\frac{t_f}{c} = \frac{1}{2}\left(1 - \frac{m_c}{m}\right)\frac{m}{\rho c} \tag{6}$$

respectively. Thus, the sheet thickness of the core and face-sheets can be expressed directly in terms of the areal mass ratios m_c/m and $m/\rho c$.

The three-point bending strength of a simply supported sandwich panel of width b, core thickness c and span $2L$ scales as

$$F_{pk} = \frac{2M_p}{L} = \frac{2\sigma_Y bct_f}{L} f_1\left(t_c, t_f, c\right) \tag{7}$$

where M_p is the plastic moment of the cross section and f_1 is a function of the cross-sectional geometry. Equation (7) can be rewritten in nondimensional form as

$$\hat{F} = \frac{F_{pk}}{\sigma_Y bc} = f_2\left(\frac{t_c}{c}, \frac{t_f}{c}, \frac{2L}{c}\right) \tag{8}$$

and using Eqs. (4)–(6), the sheet thickness ratios can be expressed as areal mass ratios giving

$$\hat{F} = \frac{F_{pk}}{\sigma_Y bc} = f_3\left(\frac{m}{\rho c}, \frac{m_c}{m}, \frac{2L}{c}\right) \tag{9}$$

Therefore, the nondimensional collapse load $\hat{F}$ is a function of the normalized span $2L/c$ and of the aerial mass ratios $m/\rho c$ and m_c/m.

In the experimental study, and associated numerical simulations reported above, the normalized span $2L/c$ was held fixed at 11.4. The mass ratios were $m/\rho c = 0.052$ and $m_c/m = 0.48$ for sandwich beams of areal mass $m = 9.1$ kg/m^2 and were $m/\rho c = 0.079$ and $m_c/m = 0.31$ for sandwich beams of areal mass $m = 13.8$ kg/m^2.

We proceed by considering the sandwich panel response for corrugated cores and Y-frame cores, first, with $m/\rho c$ held fixed at 0.052 and, second, with varying mass ratio $m/\rho c$. The simulations with $m/\rho c = 0.052$ represent the case considered in the above experimental study with $m = 9.1$ kg/m^2 and $c = 22$ mm. Simulations were performed for selected values of m_c/m in the range 0.15 to 0.95 and of normalized spans $2L/c$ in the range from 5 to 30. The overhang of the simply supported sandwich panels was $0.5L$ and the length of the face-plates added to the extremities of the sandwich panels without a back face was $0.56L$: again, these values were equal to those used in the experimental investigation, recall Fig. 5(*a*). In all cases, the central and support rollers had a diameter $D = 9$ mm, giving $D/c = 0.41$.

4.2.2 Peak Loads. The normalized peak load $\hat{F} = F_{pk}/(\sigma_Y bc)$ is plotted in Fig. 13 as a function of normalized span $2L/c$ for four selected values of m_c/m. The responses of sandwich panels with a corrugated core and a Y-frame core are shown in Fig. 13(*a*) and 13(*b*), respectively. In each plot, results are shown for sandwich panels with both faces present and for sandwich panels with the back face absent.

The peak load of all sandwich panels increases with increasing proportion of mass in the core, m_c/m. This increase in strength is more significant for short panels than for long panels. Also, with increasing m_c/m, the peak strength becomes less sensitive to whether the sandwich panel contains both face-sheets or only the front face-sheet: this is consistent with the fact that the peak

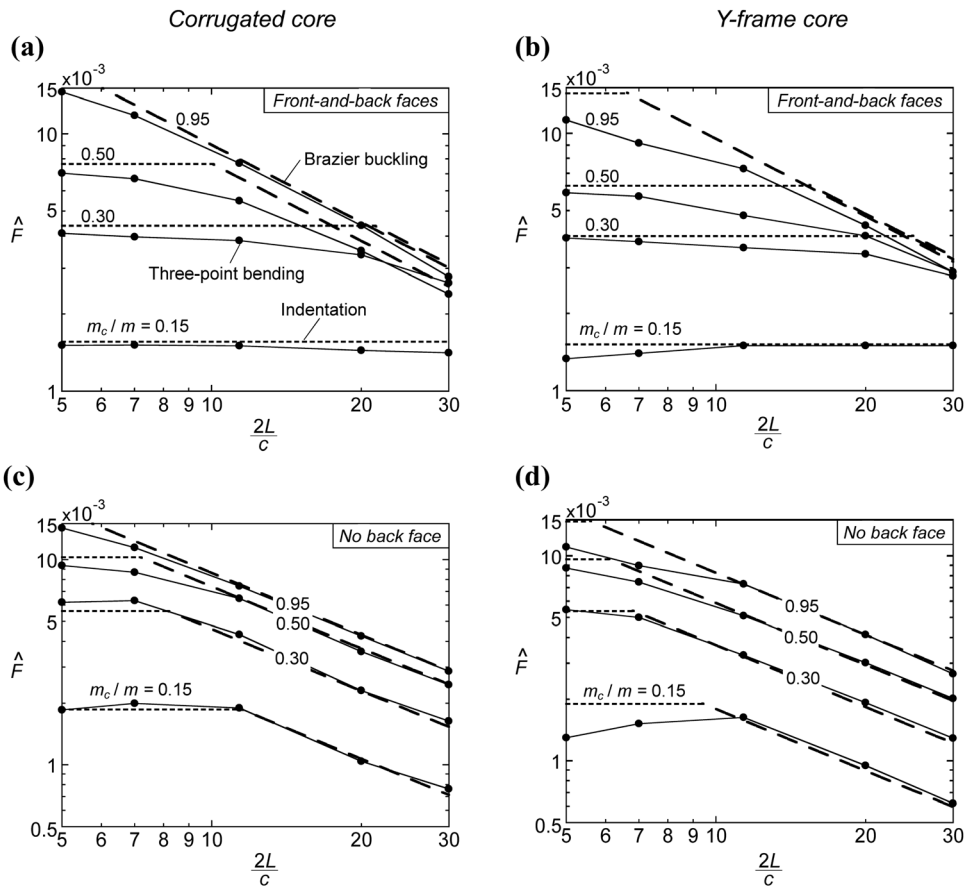

Fig. 17 Normalized peak load $\hat{F} = F_{pk}/(\sigma_Y bc)$ as a function of the normalized span $2L/c$ for simply supported sandwich panels and selected values of m_c/m ($m/\rho c = 0.052$). The three-point bending results are reproduced from Fig. 13. The indentation and Brazier buckling strengths are included as short and long dashed lines, respectively. Sandwich panels with front-and-back faces are shown with (*a*) a corrugated core and (*b*) a Y-frame core. Likewise, sandwich panels absent the back face are shown with (*c*) a corrugated core and (*d*) a Y-frame core.

strength is dominated by the presence of the core rather than the relatively thin face-sheets at high m_c/m.

Next, consider the role of the back face upon the peak strength. For $2L/c$ less than approximately 15, the sandwich panels with a front face of double thickness but absent the back face are stronger than those with front-and-back faces present. This is due to the fact that the thicker front face gives rise to a higher indentation strength. In contrast, sandwich panels with front-and-back faces have higher peak loads than panels without a back face for $2L/c > 15$; this is consistent with the fact that the Brazier buckling load is reduced when the back face is removed.

In order to determine the degree to which sandwich panel collapse is dictated by core indentation or by Brazier buckling, a series of additional calculations have been performed to obtain the collapse strength due to each of these mechanisms acting in isolation. The details are as follows.

4.2.3 Collapse Mechanisms

4.2.3.1 Indentation. The FE method was also used to obtain the indentation strength of the sandwich panels of geometry given in the previous section. To achieve this, the boundary conditions were changed such that the panel was adhered to a rigid foundation as shown in Fig. 14(*a*). This was achieved by constraining the translational degrees-of-freedom to zero along the bottom face of the panel.

Representative collapse responses of sandwich panels resting upon a rigid foundation are given in Fig. 15(*a*) for $m/\rho c = 0.052$ and $m_c/m = 0.5$. The predictions of indentation strength are limited to $2L/c = 11.4$, as used in the experimental study on sandwich beams. Results are shown for corrugated and Y-frame cores, and for sandwich panels with and without a back face. The responses exhibit a peak load F_I at a roller displacement δ of approximately 1% of the core thickness c. A small load drop ensues and subsequent deformation occurs at almost constant load. These simulations were repeated for other selected values of m_c/m and the results are summarized in Fig. 15(*b*): the normalized indentation strength $\hat{F}_I = F_I/(\sigma_Y bc)$ is plotted as a function of the proportion of mass in the core.

For all sandwich panels analyzed, the indentation strength increases with increasing m_c/m. The indentation strength is also sensitive to topology:

(i) sandwich panels with a corrugated core have higher indentation strengths than their counterparts with a Y-frame core, and
(ii) the indentation strength of panels with a double thickness front face and absent back face exceeds that of sandwich panels with front-and-back faces present. These features have already been noted above in reference to Fig. 13.

4.2.3.2 Brazier plastic buckling. The critical bending moment causing a sandwich panel to collapse by Brazier plastic buckling is also obtained with the FE method. For these simulations, all nodes (and corresponding degrees-of-freedom) at the right end of the panel are tied to a rigid surface as illustrated in Fig. 14(*b*). The rigid surface is rotated by an angle ω about the x_1-axis, with the axis of rotation positioned at mid-height of the panel. Otherwise, the rigid surface is free to translate in the x_2 and x_3 directions to ensure that no axial or transverse forces are applied to the panel. To prevent rigid body motion, the x_2- component of nodal displacement is constrained to equal zero for one node of the front face ($x_1 = 0$), at the left-hand end of the panel ($x_3 = 0$).

The representative collapse response of sandwich panels with $m/\rho c = 0.052$ and $m_c/m = 0.5$ is given in Fig. 16(*a*). Results are shown for both corrugated and Y-frame core topologies and for sandwich panels with and without a back face. As the angular displacement ω is increased, the reaction moment M increases up to a peak value M_B due to Brazier plastic buckling, and this is followed by a softening response. These simulations have been repeated for selected values of m_c/m and the normalized Brazier buckling moment $\hat{M} = M_B/(\sigma_Y bc^2)$ is plotted in Fig. 16(*b*) as a function of the proportion of m_c/m, with $m/\rho c = 0.052$. The simulations are done for sandwich panels with $2L/c = 11.4$, but the peak moment is relatively insensitive to this ratio.

It is clear from Fig. 16(*b*) that the Brazier buckling moment $\hat{M}$ for a sandwich panel, absent the back face, increases with increasing m_c/m. For these structures, the position of the neutral axis is sensitive to the proportion of mass in the core; an increase in m_c/m moves the neutral axis closer to the center of the core, increases the structural efficiency in plastic bending and leads to an increase in the Brazier buckling strength. In contrast, for sandwich panels with front-and-back faces present, the position of the neutral axis is relatively insensitive to the proportion of mass in the core and $\hat{M}$ is relatively insensitive to the value of m_c/m.

4.2.3.3 Interpretation of the three-point bending response in terms of indentation and Brazier buckling. We anticipate that, at a sufficiently short span $2L$, the three-point bending strength F_{pk} is approximated by the indentation strength F_I and is independent of span. In contrast, the three-point bending strength of long panels is dictated by Brazier plastic buckling; for a simply supported sandwich panel, the collapse load associated with Brazier plastic buckling scales with the panel length $2L$ according to:

$$F_B = \frac{2M_B}{L} \tag{10}$$

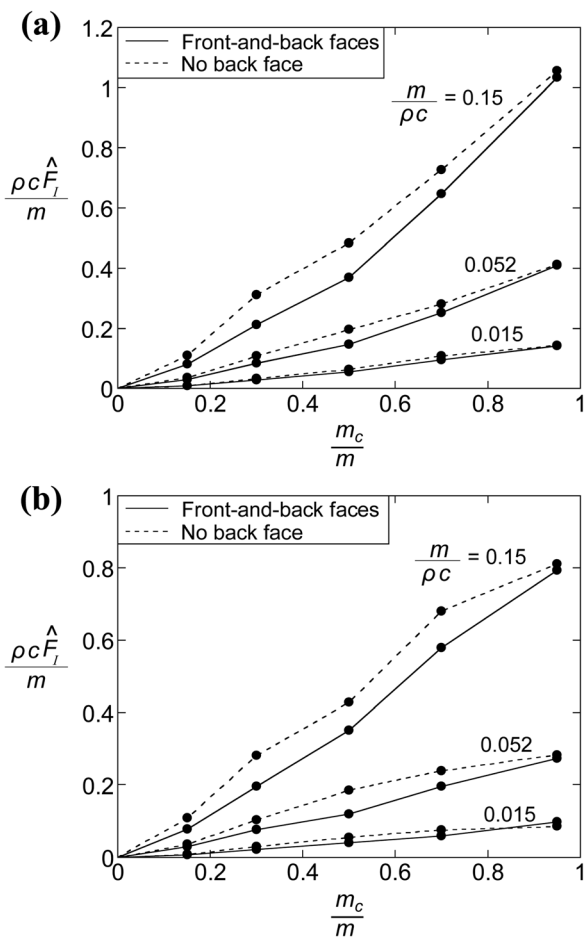

Fig. 18 Normalized indentation strength per unit mass $\rho c\hat{F}_I/m$ as a function of m_c/m for selected values of $m/\rho c$. Results are shown for sandwich panels with (*a*) a corrugated core and (*b*) a Y-frame core.

The indentation load and Brazier buckling moment, as given in Figs. 15(*b*) and 16(*b*), are now used to estimate the collapse load of a panel in three-point bending. The lower value of F_I and F_B determines which collapse mechanism is active. These asymptotic predictions of collapse load are compared with the three-point bending collapse loads in Fig. 17. Comparisons are made in Figs. 17(*a*) and 17(*b*) for sandwich panels with front-and-back faces present, and in Figs. 17(*c*) and 17(*d*) for sandwich panels with the back face absent.

In broad terms, there is excellent agreement between the predicted indentation load and the three-point bend load at short spans, and between the predicted Brazier buckling load and the three-point bend load at long spans. The deformation mode of the panels in three-point bending confirms this (not shown). The switch in response from indentation to Brazier buckling occurs at a transition value of span $2L_t/c$. For sandwich panels containing front-and-back faces, $2L_t/c$ decreases with increasing m_c/m. This is consistent with the feature that F_I increases with increasing m_c/m whereas M_B is relatively insensitive to m_c/m for panels containing front-and-back faces. In contrast, the transition span $2L_t/c$ for sandwich panels with the back face absent is only mildly influenced by the value of m_c/m. This arises from the fact that F_I and M_B both increase with increasing m_c/m for sandwich panels absent the back face.

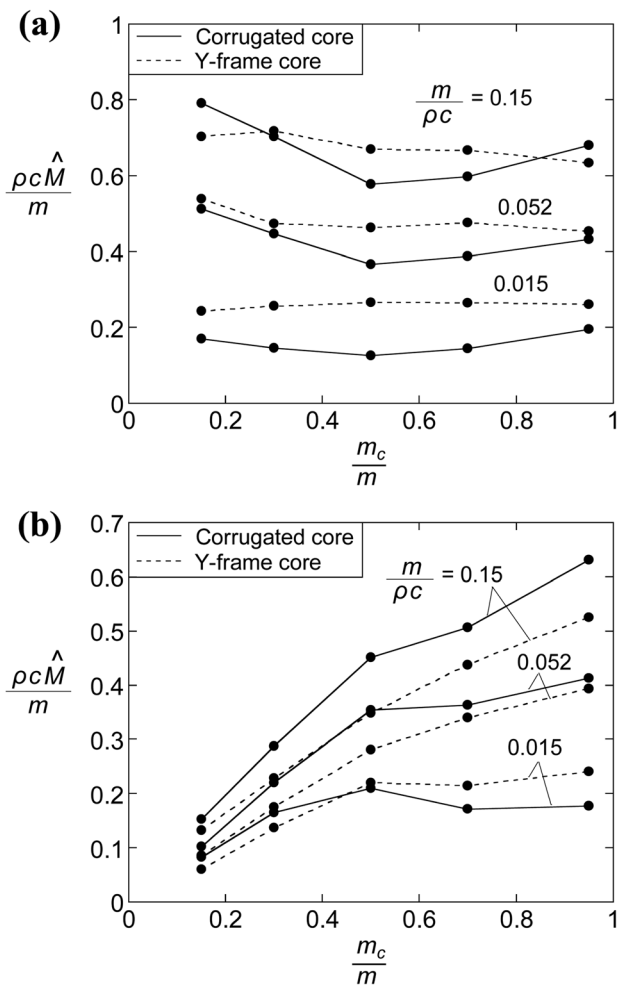

Fig. 19 Normalized Brazier buckling moment per unit mass $\rho c\hat{M}/m$ as a function of m_c/m for selected values of $m/\rho c$. Results are shown for sandwich panels (*a*) with front-and-back faces present and (*b*) without a back face.

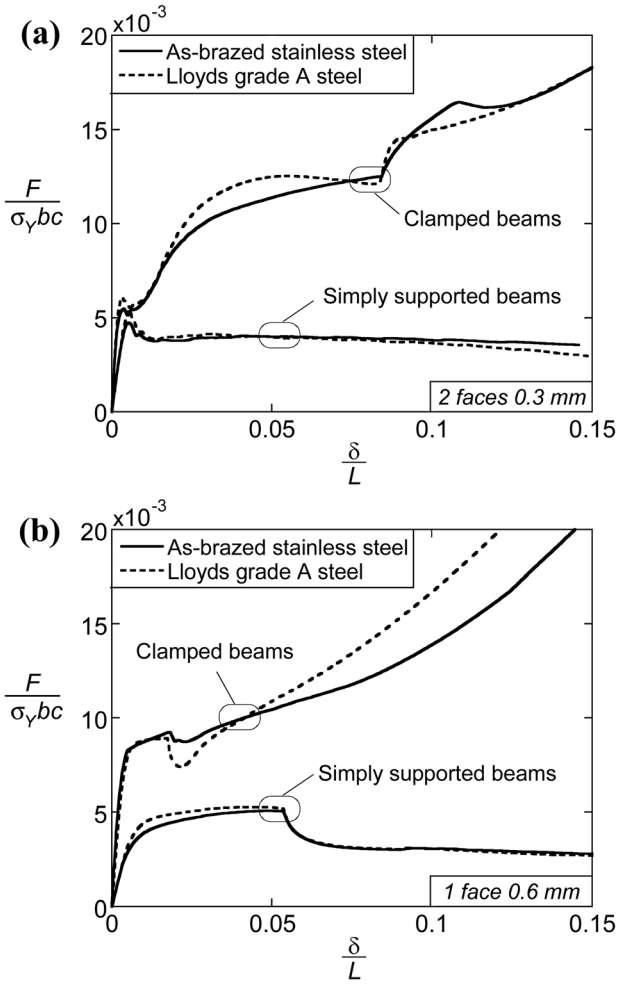

Fig. 20 Sensitivity of the three-point bending response of a sandwich beam with a Y-frame core to the choice of material. (*a*) Front-and-back faces are present and (*b*) the back face is absent.

4.2.4 Sensitivity of the Three-point Bending Strength to the Value of $m/\rho c$. It has been demonstrated above that the three-point bending strength is adequately represented by the two asymptotic behaviors of core indentation and Brazier buckling, with the operative collapse mode dictated by the beam span. We proceed to explore the dependence of the indentation strength and the Brazier buckling strength upon $m/\rho c$.

The indentation strength and Brazier buckling strength are plotted as a function of m_c/m in Figs. 18 and 19, for selected values of $m/\rho c$ in the range of 0.015 and 0.15. Indentation strengths are shown in Fig. 18(*a*) for panels with a corrugated core and in Fig. 18(*b*) for panels with a Y-frame core; in each plot, results are given for panels with both faces present, and for panels with the back face absent. For all sandwich panels considered, the normalized indentation strength per unit mass $\rho c\hat{F}_I/m$ increases with increasing value of $m/\rho c$. The observations made previously for sandwich panels with $m/\rho c = 0.052$ also hold true for other values of $m/\rho c$: (i) sandwich panels with a corrugated core have higher indentation strengths than those with a Y-frame core and (ii) relocating the back face material onto the front face increases the indentation strength of the sandwich panel.

The results for the Brazier buckling moment are given in Fig. 19(*a*) for panels with front-and-back faces present and in Fig. 19(*b*) for panels with the back face absent. In each plot, sandwich panels with a corrugated core are compared to those with a Y-frame core. The limit of m_c/m tending to zero is not included in Figs. 19(*a*) and 19(*b*) as this limit has no practical value and is

not associated with a peak moment. It is clear from Fig. 19(*a*) that the Brazier buckling moment is relatively insensitive to m_c/m when front-and-back faces are present. In contrast, when the back face is absent, the Brazier buckling strength increases with increasing m_c/m. This was observed previously for sandwich panels with $m/\rho c = 0.052$ (see Fig. 16(*b*)) but the results of Fig. 19 demonstrate that it holds true for other selected values of $m/\rho c$. Now consider the effect of $m/\rho c$ upon the normalized Brazier buckling strength per unit mass $\rho c\hat{M}/m$. Regardless of whether the back face is present or absent (and regardless of the core topology), $\rho c\hat{M}/m$ increases by a factor of about 3 when $m/\rho c$ is increased by a factor of 10 from 0.015 to 0.15.

5 Concluding Remarks

Sandwich beams with corrugated and Y-frame cores have been manufactured by brazing together AISI 304 stainless steel sheets. The dimensions of the cores were approximately 1:20 scale models of the cores used in a ship hull. In addition, the uniaxial tensile response of as-brazed stainless steel was found to be representative of shipbuilding steel up to strain levels of about 10%.

The three-point bending responses of sandwich beams with (i) front-and-back faces present and (ii) front face present, but back face absent have been measured and compared on an equal mass basis. The tests were done using simply supported and clamped boundary conditions, with the prismatic axis of the core aligned with the longitudinal axis of the beam. Sandwich beams with front-and-back faces present collapsed by indentation whereas structures without a back face collapsed by Brazier plastic buckling. Despite having different collapse mechanisms, sandwich beams with front-and-back faces and those without a back face had comparable three-point bending strengths for the choice of beam span employed.

Three-dimensional FE models were developed and the simulations were found to be in good agreement with the measured responses. The FE method was also used to study the influence of the mass distribution between the face-sheets and core. Upon concentrating the mass of the sandwich panel within the core the three-point bending strength of the structure increases. The analysis also showed the influence of the span upon the collapse response of a sandwich panel; short panels failed by indentation and long panels collapsed by Brazier plastic buckling. Sandwich panels with a corrugated core, and absent the back face have the highest indentation strength and are thereby optimal for short spans, recall Fig. 18. In contrast, it is clear from Fig. 19 that panels with front-and-back faces have greater Brazier buckling strengths than their counterparts absent the back face; consequently, panels with front-and-back faces are optimal for long spans. However, the choice of core topology plays only a minor role in the Brazier buckling regime: the corrugated core is either stronger or weaker than the Y-frame core depending upon the precise values of $m/\rho c$ and of m_c/m and upon whether the sandwich panel has the back face present or absent.

Acknowledgment

This research was carried out under the project number MC2.06261 in the framework of the Research Program of the Materials innovation institute M2i (www.m2i.nl). The authors are also grateful for the financial support of the Fonds Québécois de la Recherche sur la Nature et les Technologies (FQRNT).

Appendix: Sensitivity of the Three-Point Bending Response to the Choice of Parent Material

The influence of the parent material on the three-point bending responses of simply supported and clamped sandwich beams was investigated using the finite element (FE) method. The models used to simulate the experiments (see Sec. 2.3) were used for this analysis, except that the material properties of as-brazed stainless steel were replaced by the ones of Lloyd's grade A steel. The yield strength was taken to be $\sigma_Y = 280$ MPa and the hardening response of the material was tabulated in Abaqus from the plot given in Fig. 3. Both grades of steel have a Young's modulus of $E = 210$ GPa and a Poisson's ratio of $\upsilon = 0.3$.

The three-point bending responses of beams with a Y-frame core are compared in Fig. 20 for the two choices of material. The responses of sandwich beams with front-and-back faces are shown in Fig. 20(*a*) whereas their counterparts without a back face are shown in Fig. 20(*b*). In each figure, results are shown for both simply supported and clamped boundary conditions, and the load F has been normalized by the yield strength of the as-brazed stainless steel, $\sigma_Y = 210$ MPa. The peak load of sandwich beams made from as-brazed stainless steel are within 12% of those made from grade A steel. In general, the results in Fig. 20 indicate that the three-point bending response of a sandwich beam made from as-brazed stainless steel is representative of one made from Lloyd's grade A steel.

References

[1] Burgherr, P., 2007, "In-Depth Analysis of Accidental Oil Spills From Tankers in the Context of Global Spill Trends From all Sources," J. Hazard. Mater., **140**, pp. 245–256.

[2] Paik, J. K., 2003, "Innovative Structural Designs of Tankers Against Ship Collisions and Grounding: A Recent State-of-the-art Review," Mar. Technol., **40**(1), pp. 25–33.

[3] Wevers, L. J., and Vredeveldt, A. W., 1999, "Full Scale Ship Collision Experiments 1998," Technical Report No. 98-CMC-R1725, TNO, Delft, Netherlands.

[4] van de Graaf, B., Broekhuijsen, J., Vredeveldt, A. W., and van de Ven, A., 2004, "Construction Aspects for the Schelde Y-shape Crashworthy Hull Structure," *Proceedings of the 3rd International Conference on Collision and Grounding of Ships*, Izu, Japan, pp. 229–233.

[5] Rubino, V., Deshpande, V. S., and Fleck, N. A., 2008, "The Collapse Response of Sandwich Beams With a Y-frame Core Subjected to Distributed and Local Loading," Int. J. Mech. Sci., **50**(2), pp. 233–246.

[6] Côté, F., Deshpande, V. S., Fleck, N. A., and Evans, A. G., 2006, "The Compressive and Shear Responses of Corrugated and Diamond Lattice Materials," Int. J. Solids Struct., **43**(20), pp. 6220–6242.

[7] Valdevit, L., Wei, Z., Mercer, Z., Zok, F. W., and Evans, A. G., 2006, "Structural Performance of Near-Optimal Sandwich Panels With Corrugated Cores," Int. J. Solids Struct., **43**(16), pp. 4888–4905.

[8] Rubino, V., Deshpande, V. S., and Fleck, N. A., 2010, "The Three-Point Bending of the Y-frame and Corrugated Core Sandwich Beams," Int. J. Mech. Sci., **52**(3), pp. 485–494.

[9] Broekhuijsen, J., 2003, "Ductile Failure Criteria and Energy Absorption Capacity of the Y-shape Test Section," M. Sc. thesis, TU Delft, Delft, The Netherlands.

[10] Dassault Système Simulia Corp., 2009, *Abaqus Analysis User's Manual*, Version 6.9, Providence, RI.

[11] Brazier, L. G., 1927, "On the Flexure of Thin Cylindrical Shells and Other 'Thin' Sections," Proc. R. Soc. A, **116**, pp. 104–114.